DoA Estimation Using Compact CRLH Leaky-Wave Antennas: Novel Algorithms and Measured Performance

Henna Paaso, Nikhil Gulati, *Member, IEEE*, Damiano Patron, *Member, IEEE*, Aki Hakkarainen, Janis Werner, Kapil R. Dandekar, *Senior Member, IEEE*, Mikko Valkama, *Senior Member, IEEE*, and Aarne Mämmelä, *Senior Member, IEEE*

Abstract—Traditional direction-of-arrival (DoA) estimation algorithms for multielement antenna arrays (AAs) are not directly applicable to reconfigurable antennas due to inherent design and operating differences between AAs and reconfigurable antennas. In this paper, we propose novel modifications to the existing DoA algorithms and show how these can be adapted for real-time DoA estimation using two-port composite right/ left-handed (CRLH) reconfigurable leaky-wave antennas (LWAs). First, we propose a single/two-port multiple signal classification (MUSIC) algorithm and derive the corresponding steering vector for reconfigurable LWAs. We also present a power pattern cross correlation algorithm that is based on finding the maximum correlation between the measured radiation patterns and the received powers. For all algorithms, we show how to simultaneously use both ports of the two-port LWA in order to improve the DoA estimation accuracy and, at the same time, reduce the scanning time for the arriving signals. Moreover, we formulate the Cramer-Rao bound for MUSICbased DoA estimation with LWAs and present an extensive performance evaluation of MUSIC algorithm based on numerical simulations. In addition, these results are compared to DoA estimation with conventional AAs. Finally, we experimentally evaluate the performance of the proposed algorithms in an indoor multipath wireless environment with both line-of-sight (LoS) and non-LoS components. Our results demonstrate that DoA estimation of the received signal can be successfully performed using the two-port CRLH-LWA, even in the presence of severe multipath.

Manuscript received August 1, 2016; revised March 20, 2017; accepted June 4, 2017. Date of publication July 13, 2017; date of current version September 1, 2017. This work was supported in part by the VTT Technical Research Center of Finland and the Finnish Funding Agency for Technology and Innovation within the framework of the Reconfigurable Antenna-Based Enhancement of Dynamic Spectrum Access Algorithms project, in part by the Doctoral Program of the President of Tampere University of Technology, in part by the Academy of Finland under Grant 288670, and in part by the U.S. National Science Foundation as part of the Wireless Innovation between Finland and United States partnership under Grant CNS-1147838. (Corresponding author: Henna Paaso.)

- H. Paaso and A. Mämmelä are with the VTT Technical Research Center of Finland, 90570 Oulu, Finland (e-mail: henna.paaso@vtt.fi; aarne.mammela@vtt.fi).
- N. Gulati is with General Electric, San Ramon, CA 95134 USA (e-mail: nikhil.gulati@ge.com).
- D. Patron and K. R. Dandekar are with the Department of Electrical and Computer Engineering, Drexel University, Philadelphia, PA 19104 USA (e-mail: damiano.patron@gmail.com; dandekar@drexel.edu).
- A. Hakkarainen, J. Werner, and M. Valkama are with the Department of Electronics and Communications Engineering, Tampere University of Technology, 33720 Tampere, Finland (e-mail: aki.hakkarainen@tut.fi; janis.werner@tut.fi; mikko.e.valkama@tut.fi).

Digital Object Identifier 10.1109/TAP.2017.2724584

Index Terms—Cramer—Rao bound (CRB), directional antennas, direction-of-arrival (DoA) estimation, leaky-wave antennas (LWAs), measurements, multiple signal classification (MUSIC).

I. INTRODUCTION

DAPTIVE antenna systems have gained significant attention for potential use in next generation wireless systems. These antennas have been shown to provide additional gains in both single user [1]–[3] and multiuser [4], [5] multiple-input multiple-output (MIMO) systems. They have also been shown to be useful for applications such as positioning for user tracking and location-based services in WiFi networks [7] and localization [6].

Adaptive antenna systems can steer the main beam to a desired direction while spatially nulling the power in undesired directions to avoid interference [8]. Direction-of-arrival (DoA) estimation algorithms have played an important role in the practical implementation of antenna arrays (AAs) [9], and the importance of DoA estimation and directional communications will even be emphasized in the future networks. For instance, 5G ultradense networks are expected to consist of access nodes with roughly 50-m intersite distances outdoors [10], which consequently increase the probability of line-of-sight (LoS) conditions approximately to 70% [11], [12]. Thus, the significance of spatial directions and estimated DoAs will obviously be higher than in the conventional radio networks. In addition to spectrum reuse and interference avoidance, estimated DoAs can be used for device localization. An example of localization using sectorized antennas and an antenna model that is also valid for leaky-wave antennas (LWAs) can be found in [13].

Adaptive antennas can be categorized into two classes: 1) phased arrays and 2) reconfigurable antennas. Traditionally, phased array systems use an array of many elements to control the beam direction and radiation pattern shape [14], [15], resulting in very large form factors, e.g., at WiFi frequency bands. Due to these form-factor limitations, beamforming and DoA estimation techniques are more feasible to deploy in the case of large base station devices [16]. In contrast to large AAs, the class of composite right/left-handed (CRLH) reconfigurable LWAs [17] does not require multielement AAs or feeding networks [18]. In practical scenarios, LWAs have many other advantages. The first advantage of

0018-926X © 2017 IEEE. Personal use is permitted, but republication/redistribution requires IEEE permission. See http://www.ieee.org/publications_standards/publications/rights/index.html for more information.

the LWAs is the wide spatial direction range in beamsteering. In [19] and [20], a planar phased array hardly reaches \pm 40° while LWAs can easily steer the beam up to \pm 60°. The second benefit is the cost: a single LWA costs much less in terms of substrate area and a number of lumped components with respect to a phased array that uses multiple antenna elements with each antenna element connected to a radio frequency (RF) converter and an analog-to-digital (A/D) converter. In addition, LWAs have a low dc power consumption. The third advantage is the small size of the antenna: the minor printed circuit board area required by an LWA as opposed to a phased-array designed at the same frequency. Finally, there has been increased academic [3]-[5], [17], [22] and industrial interests [23] in traveling wave antenna technologies. By considering these advantages, particularly compactness and beamsteering, CRLH-LWAs have a great potential to be used in DoA estimation systems.

Several DoA estimation algorithms for conventional AAs have been proposed in [24]–[28]. However, these conventional algorithms cannot be directly used for DoA estimation and beamforming using CRLH-LWAs due to the inherent difference in design and operation of the LWAs versus traditional AAs. The reason for this difference is that using an LWA, only a single observation is available at each sampling instance, unlike in conventional AAs where signals can be observed from different elements of the AA [29]. For example, the conventional multiple signal classification (MUSIC) algorithm generates a spatial correlation matrix of the signal samples received from the elements of an AA [24]. In addition, the performance of this algorithm is noticeably influenced by different array characteristics, for example, a number of elements, array geometry, and the mutual coupling interactions between AA elements [30], [31]. These problems can potentially be avoided or reduced using the CRLH-LWA. Due to the inherent difference in design of the CRLH-LWA, our single/two-port MUSIC algorithm uses M received signals—each obtained with a different radiation pattern—that are measured from two antenna ports. Then, a correlation matrix can be formed using these M received signals, as discussed preliminarily in [32].

There are only a limited number of papers where DoA estimation algorithms are proposed for LWAs. In [7], an energy-based DoA estimation system is evaluated at a fixed frequency employing a CRLH-LWA. In [33], the DoA of the wideband pulsed signal is estimated from the cross-correlation coefficients using the received spectra of the antenna with a predetermined incident angle-dependent spectra. DoA estimators that assume a noncooperative transmitter (TX) and that are applicable to sectorized antennas, such as an LWA, are proposed in [34]. Similar work for DoA estimation has also been reported independently in [35] and [36] that use the MUSIC algorithm for CRLH-LWA. In [35], only experimental results are presented and it is not shown how the MUSIC algorithm can be formulated using LWAs. Furthermore, Vakilian et al. [35], [36] introduce only experimental studies of MUSIC algorithm in an anechoic chamber and the antenna uses only one antenna port at a time. Further, in [37] and [38], reactance domain MUSIC [37] and unitary MUSIC [38] algorithms for electronically steerable parasitic array radiator (ESPAR) antennas are introduced. In all these papers, the DoA estimation was performed using a single port antenna.

In this paper, we formulate and analyze the experimental performance of two modified DoA estimation algorithms with a two-port CRLH-LWA:

- 1) single/two-port MUSIC;
- 2) power pattern cross correlation (PPCC).

In addition, the performance of these two algorithms is qualitatively compared to a low-complexity power detector (PD). In order to assess the performance of the MUSIC algorithm, we first formulate the respective Cramer–Rao bound (CRB), simulate the performance of the estimators, and compare the estimators to the CRB. Finally, these results are also compared to DoA estimation performance with AAs.

In [32] and [39], we presented the performance of the single/two-port MUSIC algorithm in an anechoic chamber. In contrast to these studies and other DoA estimation techniques in [34]–[38], we explore, in this paper, the DoA estimation capabilities of a two-port CRLH-LWA in a real-world multipath indoor environment and using both antenna ports at the same time. Thus, we also take advantage of the beam symmetry characteristic of LWAs by steering bi-directional beams. As a result, the overall signal acquisition and estimation time are halved, and the length of the periodical training sequence can be truncated. In addition, the algorithms can also be used in MIMO systems.

This paper is organized as follows. Section II introduces a detailed description of the CRLH-LWA design. Section III presents the DoA estimation algorithms for a compact CRLH-LWA. Analytical performance bound and simulation-based algorithm performance evaluations are presented in Section IV. In Sections V and VI, the experimental setup and measurement results are described and analyzed, respectively. Finally, conclusions are drawn in Section VII.

Notation: We use capital bold letters to denote matrices and small bold letters for vectors. \mathbf{H}^{-1} , \mathbf{H}^{\dagger} , and \mathbf{H}^{T} denote the matrix inverse, Hermitian and transpose operation, respectively. The complex conjugate is denoted by $(\cdot)^*$. For deterministic signals s(k), the expectation operator is defined as in [42], i.e., $\mathrm{E}[s(k)] = \lim_{N \to \infty} 1/N \sum_{k=1}^{N} s(k)$. Given a real-valued quantity x, $y = \lfloor x \rfloor$ denotes the closest integer such that $y \leq x$.

II. COMPOSITE RIGHT/LEFT-HANDED LEAKY-WAVE ANTENNAS

LWAs are a class of radiating elements based on the concept of the traveling-wave behavior [17]. As opposed to conventional resonating-wave antennas, when an RF signal is applied to the LWA's input port, the traveling wave progressively leaks out energy as it travels along the waveguide structure. The radiated beam will exhibit a main lobe normal to the plane of the antenna with directivity strictly related to the leakage phenomenon.

The reconfigurable CRLH antenna is a periodic LWA structure made by a cascade of metamaterial unit cells [21]. The unit cell is designed in such a way that the propagation constant β sweeps within the radiated region of the dispersion

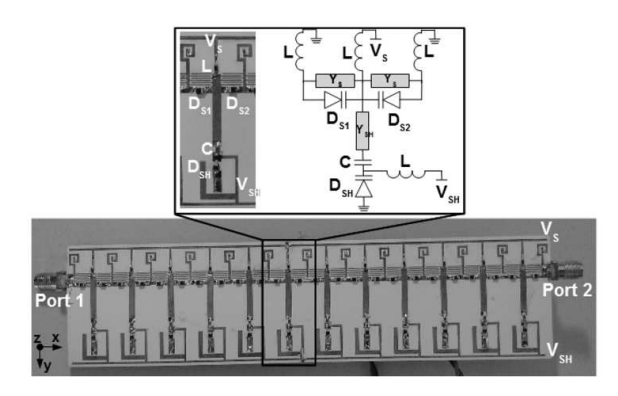


Fig. 1. Picture of the fabricated CRLH-LWA, with the details of a single unit cell and relative circuit model.

curve: $|\beta| < k_0$ where k_0 is the free space wavenumber [17]. Each unit cell is populated with two varactor diodes in series and one in shunt configuration. The CRLH behavior is determined by designing the unit cell with proper series capacitance (Y_S) and shunt inductive component (Y_{SH}) through a microstrip stub. The propagation constant β along the waveguide structure can be electronically modulated from lefthand $(\beta < 0)$ to right-hand $(\beta > 0)$ regions through the two dc voltages V_S and V_{SH} . As depicted in the inset of Fig. 1, two series varactors D_{S1} and D_{S2} are controlled by the voltage V_S , which is provided through folded microstrip inductor and lumped inductor L = 220 nH. The shunt component is varied through the varactor D_{SH} that is controlled by the voltage $V_{\rm SH}$, applied by means of a microstrip open stub. A C = 0.5 pF capacitor is used to decouple the two dc voltages. As a result, these variations of the wave propagation characteristic are responsible for steering the beam. Note that the LWA consists of multiple cascaded unit cells and operates as a single antenna entity whose beam is steered by tuning the control voltages. This is a very fundamental difference compared to multielement AAs where the signals can be observed and processed from different RF branches and eventually combined after phase shifting.

In order to achieve the maximum beam coverage by switching between the two input ports, we have optimized the design within the left-hand region ($\beta < 0$). In other words, when port 1 is used the beam can be steered from 0° to -60° , while switching to port 2 the beam covers the symmetrical quadrant from 0° to $+60^{\circ}$ as illustrated at the LWA sketch in Fig. 2. The beam can be electronically steered from broadside $\theta_1 = \theta_2 = 0^{\circ}$ to off-broadside directions: to the left when $\theta_1 < 0^{\circ}$ and to the right when $\theta_2 > 0^{\circ}$ [17]. The relationship between propagation constant β and the beam steering angle θ can be expressed as

$$\theta_1 = \arcsin\left(\frac{\beta}{k_0}\right), \quad \beta < 0$$

and

$$\theta_2 = \arcsin\left(\frac{\beta}{k_0}\right), \quad \beta > 0.$$
 (1)

In order to reduce the antenna form factor and enhance the radiation efficiency, we selected a 1.6-mm-thick Rogers 4360 substrate, characterized by a relatively high dielectric

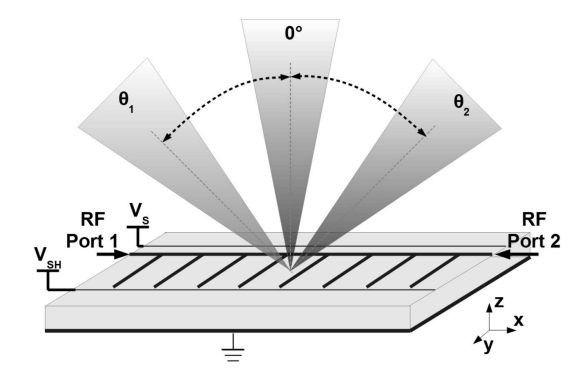


Fig. 2. Sketch of a two-port CRLH-LWA and an example of beam steering capabilities from broadside 0° to off-broadside directions: to the left θ_1 and to the right θ_2 .

constant $\epsilon_r = 6.15$ and low loss tangent = 0.003. The single unit cell, as well as the overall structure, was designed using a full-wave simulator and tuned to operate within the entire 2.4-GHz 802.11 WiFi band. In LWAs, the directivity of the radiated beam is directly proportional to the number of cascaded unit cells. In our design, we choose to cascade N = 12 unit cells in order to keep an overall small form factor while preserving a good radiated gain, on the order of 5 dBi. Unlike, the previous LWA models [22] where the dc bias was provided using long $\lambda/4$ microstrip transformers, the use of lumped and folded solutions allows for a further size reduction of the LWA design. The resulting dimensions of the milled prototypes are 156 mm in length and 38 mm in height.

Radiation pattern measurements at the frequency of 2.46 GHz were carried out within the anechoic chamber facility. As shown in Fig. 3, each radiation pattern was taken with 1° resolution and the measured gain is 4 to 5 dBi. A slight gain reduction occurs for angles above $\theta=\pm 50^\circ$ due to the natural CRLH behavior for which the propagation constant β starts to leave the radiated region approaching the propagated regime. Each beam can be generated individually or, when using both ports, the positive (dashed line) and negative symmetric beams (solid line) will exist at the same time.

Comprehensive input impedance characterization was performed using a vector network analyzer, measuring return loss as well as isolation of the two LWA ports. The return loss curves S_{11} and S_{22} describe the impedance matching between a 50- Ω feed line and the two antennas' input ports. As depicted in Fig. 3, both input ports exhibit a -10-dB bandwidth greater than 100 MHz, ensuring good impedance matching from 2.4 to 2.5 GHz with all control voltages. On the other hand, the curve S_{21} determines the isolation between the two LWA ports and for all the configurations the values fall below -15 dB. Such a relatively high isolation allows the LWA to be effectively used as a two-element AA in a 2×2 MIMO system.

In our analysis, we exploit the additional feature of beam symmetry in LWAs, i.e., when both antenna ports are used and the antenna generates two symmetrical beams with respect to the broadside $\theta=0^\circ$ direction. For example, if $V_{\rm S}$ and $V_{\rm SH}$ are set for a 60° configuration and both RF ports are used simultaneously, the resulting beam exhibits two main lobes at

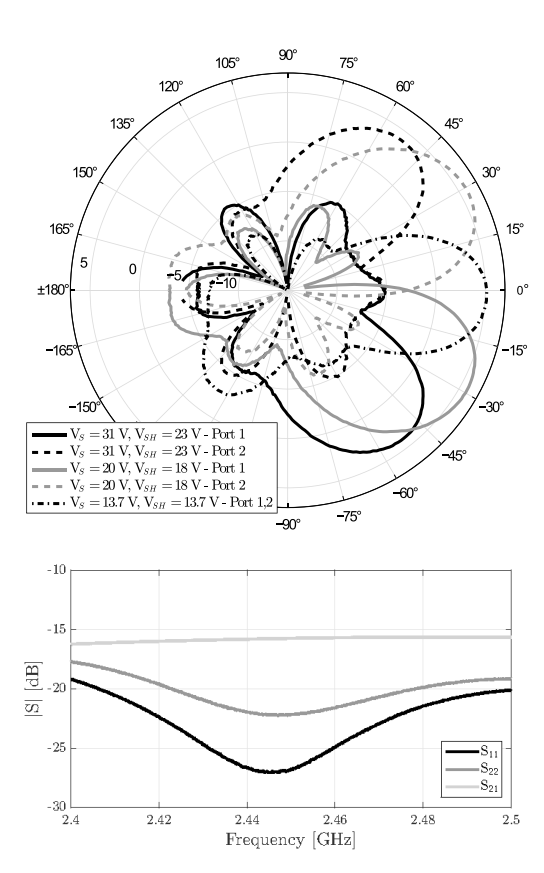


Fig. 3. Measured radiation patterns at 2.46 GHz and an example of the measured scattering parameters when $V_S=20~\mathrm{V}$ and $V_{SH}=18~\mathrm{V}$.

 $+60^{\circ}$ and -60° . In the next section, we will show that this feature can significantly decrease the processing time during the DoA estimation.

III. MODIFIED DoA ESTIMATION ALGORITHMS FOR COMPACT CRLH-LWA

In this section, we present three different DoA estimators specifically designed for LWAs: a modified single/two-port MUSIC, the PD, and the PPCC algorithm. The first algorithm is variant of the popular MUSIC algorithm that we have modified to work with LWAs, while the last two algorithms are based on evaluating the received powers for different voltage sets. The algorithms are meant to work with microstrip LWAs, but any other LWA structure, such as nonmicrostrip LWA, can also take advantage of them as long as the antennas are electronically reconfigurable. In the following sections, we will be using φ to denote the DoA and $\hat{\varphi}$ an estimate thereof.

A. Single/Two-Port MUSIC Algorithm

Conventionally, the MUSIC algorithm [24] calculates the spatial correlation matrix using the signals received by multiple elements. In this section, we show how the spatial capabilities of the conventional AA can be virtually generated with the CRLH-LWA and how the correlation matrix can be calculated when using the two-port LWA.

The first step is to measure the same transmitted signal u(k), M times through M different beams. In this way, we can

recreate spatial diversity due to M observations of the same signal but with different radiation patterns. Using both ports of the LWA simultaneously, we can receive two signals, namely, $y_1(k)$ and $y_M(k)$, at a time from two symmetrical directions. Consequently, the time for the signal repetition is halved compared to the work in [32] and [39]. With the LWAs, the $M \times 1$ received signal vector $\mathbf{v}(k)$ can be defined as

$$\mathbf{y}(k) = \mathbf{a}(\varphi)u(k) + \mathbf{z}(k) \tag{2}$$

where k is the received symbol index, $\mathbf{z}(k)$ denotes an $M \times 1$ additive white Gaussian noise vector where the elements have variance equal to σ^2 , and $\mathbf{a}(\varphi)$ is the $M \times 1$ steering vector. The mth element of the steering vector can be expressed as

$$a_m(\varphi) = \sqrt{G_m'} \sum_{n=1}^N I_n \exp[j(n-1)k_0 d(\sin(\varphi) - \sin(\theta_m))]$$
(3)

with m = 1, ..., M and

$$G'_{m} = \frac{G_{m}}{\left(\sum_{n=1}^{N} I_{n}\right)^{2}} \tag{4}$$

where G_m is the measured antenna gain (in linear scale) of set m, φ is the angular direction of the received signal, θ_m is the main beam direction of the LWA with control voltage set m, and $I_n = I_0 \exp[-\alpha(n-1)d]$ is an exponential function with a leakage factor α . The initial value of the exponential function $I_0 = 1$, with structure period d [17]. Note that the normalization (4) results in maximum gains that are exactly the same as the measured maximum gains.

The MUSIC algorithm is based on the noise subspace analysis. In order to find the noise subspace matrix, we first need to estimate the covariance matrix from the received signal. The estimated covariance matrix can be presented as

$$\hat{\mathbf{R}}_{yy} = \frac{1}{N_s} \sum_{k=1}^{N_s} \mathbf{y}(k) \mathbf{y}^{\dagger}(k)$$
 (5)

where N_s denotes the number of samples. Then, the covariance matrix is decomposed by the eigenvalue decomposition (EVD), resulting in

$$\hat{\mathbf{R}}_{yy} = \hat{\mathbf{E}}_{s} \hat{\Lambda}_{s} \hat{\mathbf{E}}_{s}^{H} + \hat{\mathbf{E}}_{n} \hat{\Lambda}_{n} \hat{\mathbf{E}}_{n}^{H}. \tag{6}$$

Here, $\hat{\mathbf{E}}_s = [\hat{\mathbf{e}}_1, \hat{\mathbf{e}}_2, \dots, \hat{\mathbf{e}}_L]$ includes the estimated eigenvectors for the signal subspace, $\hat{\Lambda}_s = \mathrm{diag}[\hat{\lambda}_1, \hat{\lambda}_2, \dots, \hat{\lambda}_L]$ is a diagonal matrix of the largest estimated eigenvalues, and L is the number of incident sources. In addition, $\hat{\mathbf{E}}_n = [\hat{\mathbf{e}}_{L+1}, \hat{\mathbf{e}}_{L+2}, \dots, \hat{\mathbf{e}}_M]$ is the noise subspace matrix and $\hat{\Lambda}_n = \mathrm{diag}[\hat{\lambda}_{L+1}, \hat{\lambda}_{L+2}, \dots, \hat{\lambda}_M]$ is the diagonal matrix of M-L noise eigenvalues. Once the eigenvectors of the noise subspace are estimated, the MUSIC pseudospectrum can finally be generated as

$$P_{\text{MUSIC}}(\theta) = \frac{\mathbf{a}^{\dagger}(\theta)\mathbf{a}(\theta)}{\mathbf{a}^{\dagger}(\theta)\hat{\mathbf{E}}_{n}\hat{\mathbf{E}}_{n}^{\dagger}\mathbf{a}(\theta)}.$$
 (7)

The DoA is then estimated as the angle where the pseudospectrum $P_{\text{MUSIC}}(\theta)$ attains its maximum, that is

$$\hat{\varphi}_{\text{MUSIC}} = \underset{\theta}{\text{arg max }} P_{\text{MUSIC}}(\theta). \tag{8}$$

B. Power-Based DoA Estimators

In this section, we introduce the PD and PPCC algorithms. Both of these algorithms are based on the received powers, which are calculated as

$$P_m = \frac{1}{N_s} \sum_{k=1}^{N_s} |y_m(k)|^2 \tag{9}$$

for every voltage set m where m = 1, ..., M.

1) Power Detector: First, we present the simple PD that is based on finding the maximum received power. However, due to varying gains for different voltage sets, we first normalize each power yielding the gain-normalized powers $\overline{P}_m^g = P_m/G_m$. The PD then obtains the DoA estimate as

$$\hat{\varphi}_{PD} = \left\{ \theta_m | m = \underset{m}{\arg \max} \overline{P}_m^g \right\}. \tag{10}$$

Obviously, the complexity of the PD is very low. However, the resolution of the algorithm is also very coarse and ultimately limited by the number of control voltage sets M.

2) Power Pattern Cross Correlation Algorithm: PPCC, which was introduced for ESPAR antennas in [40], calculates the cross-correlation coefficient between the measured powers (9) and the measured radiation patterns, $D_m(\theta)$, m = 1, ..., M for several directions θ . In this paper, we show how to apply PPCC to LWAs. Toward that end, we first normalize the measured radiation pattern D_m of each voltage set m according to

$$\overline{D}_m(\theta) = \frac{D_m(\theta)}{\sqrt{\sum_{l=1}^M D_l^2(\theta)}}.$$
(11)

Next, we calculate the normalized received powers given by

$$\overline{P}_{m} = \frac{P_{m}}{\sqrt{\sum_{l=1}^{M} P_{l}^{2}}}.$$
(12)

Thereafter, the cross-correlation coefficient is obtained as

$$\Gamma(\theta) = \sum_{m=1}^{M} \overline{P}_m \overline{D}_m(\theta). \tag{13}$$

Finally, the DoA is estimated as the angle that maximizes (13), that is

$$\hat{\varphi}_{PPCC} = \underset{\theta}{\arg\max} \Gamma(\theta). \tag{14}$$

PPCC yields more accurate DoA estimates than the PD. However, the cost of the cross-correlation computation increases with the resolution of θ . Thus, the complexity of PPCC is larger than that of the PD. Compared with the MUSIC algorithm, on the other hand, PPCC has a much lower complexity, since PPCC neither relies on EVD nor on computationally intensive matrix multiplications.

IV. ANALYTICAL PERFORMANCE BOUND AND ALGORITHM PERFORMANCE

In this section, we first formulate the CRB on MUSIC DoA estimation with LWAs. Thereafter, we compare DoA estimation with LWAs to DoA estimation with AAs in terms of the analytical CRBs and simulated performance.

A. Cramer-Rao Bound

The CRB is a lower bound on the variance of any unbiased estimator. In general, the CRB is derived as the inverse of the Fisher information matrix [41]. However, in this paper, we will use related work as the basis for our CRB formulation such that we do not have to derive the CRB from scratch. Toward that end, we refer to the seminal work [42] that deals, among other things, with the CRB on a set of estimation problems encountered in array signal processing. For n' signals impinging on an AA of m' elements, the signal model in [42] is written as

$$\mathbf{y}'(t') = \mathbf{A}'(\boldsymbol{\theta}')\mathbf{x}'(t') + \mathbf{e}'(t'), \quad t = 1, 2, ..., N$$
 (15)

where $\mathbf{v}'(t') \in \mathbb{C}^{m' \times 1}$ is the received signal vector, $\mathbf{x}'(t') \in$ $\mathbb{C}^{n'\times 1}$ is the vector of impinging signals, $\mathbf{e}'(t')$ is additive noise, and $\mathbf{A}'(\boldsymbol{\theta}') = [\mathbf{a}'(\omega_1') \dots \mathbf{a}'(\omega_{n'}')] \in \mathbb{C}^{m' \times n'}$ is a matrix composed of the steering vectors $\mathbf{a}'(\omega_i')$, i = 1, ..., n', which are a function of the parameter ω'_i that we want to estimate. In this paper, we consider only a single impinging signal, thus n'=1, i.e., $\mathbf{x}'(t')$ reduces to a scalar, $\mathbf{A}'(\vartheta')=\mathbf{a}(\omega_1')$, and we estimate only a single parameter ω'_1 . Comparing next our MUSIC signal model (2) with (15), we notice that they are in fact structurally identical if we set m' = M, t' = k, $\mathbf{y}'(t') =$ $y(k), \omega'_1 = \varphi, a'(\omega'_1) = a(\varphi), x'(t') = x(k), \text{ and } e'(t') = z(k).$ In the derivation of the CRB in [42], it is only assumed that x'(t') is deterministic, but unknown to the receiver (RX). While all the elements of y'(t') in (15) originate from the exact same moment in time, the elements of y(k) in the LWA-based model in (2) originate from M/2 different moments in time. However, under the assumptions made in Section III, these two signal models are structurally identical, and thus the signal model and assumptions in [42] are indeed compatible with our problem formulation. Consequently, we can formulate the CRB for the MUSIC algorithm with LWAs based on [42] as

$$CRB(\varphi) = \frac{\sigma^2}{2N_s \,\tilde{P}_u h(\varphi)} \tag{16}$$

with

$$h(\varphi) = ||\mathbf{a}_{\varphi}||^{2} \left(1 - \frac{|\mathbf{a}_{\varphi}^{H} \mathbf{a}|^{2}}{||\mathbf{a}_{\varphi}||^{2}||\mathbf{a}||^{2}} \right) = ||\mathbf{a}_{\varphi}||^{2} g(\varphi) \quad (17)$$

and $\tilde{P}_u = (1/N) \sum_{k=1}^{N_s} |u(k)|^2$. In (16) and (17), $\mathbf{a}_{\varphi} = (\partial \mathbf{a}/\partial \varphi)$ stands for the derivative of the steering vector with respect to the DoA, where the elements become

$$\frac{\partial a_m}{\partial \varphi} = jk_0 d\sqrt{G'_m} \sum_{n=1}^N [(n-1)I_n \cos \varphi \times \exp[j(n-1)k_0 d(\sin \varphi - \sin \theta_m)]]$$
(18)

for the LWA for which a_m is given in (3).

B. Comparison to Antenna Arrays: CRB and Performance Simulations

In this section, we compare the DoA estimation with the LWA to the DoA estimation with AAs in terms of the CRB and simulated performance. Toward that end, we first note that the DoA estimation CRB for AAs is also given by (16) when

replacing **a** with the corresponding steering vector for AAs. In this comparison, we will consider a linear AA since it is structurally similar to the considered LWA. For a linear array with M_A elements, the elements of the $M_A \times 1$ steering vector are given by

$$a_{A,m} = \exp[j(m-1)k_0d_A\sin(\varphi)] \tag{19}$$

where d_A is the spacing of the antenna elements. Correspondingly, the derivative of the steering vector with respect to the DoA is given by

$$[a_{A,m}]_{\varphi} = j(m-1)k_0 d_A \cos(\varphi) \exp[j(m-1)\kappa d_A \sin(\varphi)]. \tag{20}$$

The LWA considered in this paper, and also used in later sections for actual RF measurements, has a length of l =156 mm. For a fair comparison, the AA should have a comparable length. In order to achieve this size constraint, we have two options. First, we can fix the spacing between the antenna elements d_A and adjust the number of antenna elements $M_A = \lfloor l/d_A \rfloor + 1$. Alternatively, we can fix M_A and adjust $d_A = l/(M_A - 1)$. Now, regarding the choice of d_A , we have to make sure that we fulfill the spatial sampling theorem for linear arrays, i.e., $d_A \leq 0.5\lambda$. Commonly, the spacing is chosen such that $d_A = 0.5\lambda$. This choice has the advantage that the DoA CRB (16) is minimized (given the constraint from the sampling theorem) as can be easily verified when noting that $||\mathbf{a}||^2$ is independent of d_A , whereas $||\mathbf{a}_{\varphi}||^2$ and $|\mathbf{a}_{\varphi}^{H}\mathbf{a}|^{2}$ are proportional to d_{A}^{2} such that the CRB is inversely proportional to d_A^2 . In our comparison, we therefore consider the following two cases for the AA:

- 1) "Optimal" $d_A = 0.5\lambda \approx 60$ mm, resulting in $M_A = 3$.
- 2) $M_{\rm A}=12$ antenna elements (comparable to the N=12 unit cells of the LWA), resulting in $d_{\rm A}\approx 0.12\lambda\approx 14$ mm.

We reference these cases by referring to the respective M_A , i.e., $M_A = 3$ denotes the first case and $M_A = 12$ denotes the second case.

In order to enable a fair comparison of the LWA to the AAs, let us define the signal power P_u as the power that we would measure after receiving the signal with a unity-gain isotropic antenna, i.e., P_u is simply the power of u(k). In our simulations, we then define the signal-to-noise ratio (SNR) that we would measure after reception with the isotropic antenna as

SNR =
$$\frac{E[u(k)u^*(k)]}{E[z_i(k)z_i^*(k)]} = \frac{P_u}{\sigma^2}$$
 (21)

where $z_i(k)$ is an arbitrary element from $\mathbf{z}(k)$ (assuming that the elements are iid).

In the simulations, we generate a received signal according to the signal model (2). We use orthogonal frequency-division multiplexing (OFDM) with 48 active subcarriers as the physical (PHY) signal waveform. To match the simulation-based experiments with the used LWA, the antenna is selected to have 6 modes with the 12 main beam directions $\theta_m = \pm 10^{\circ}, \pm 20^{\circ}, ..., \pm 60^{\circ}$. For steering vector generation, we use the measured antenna gains G_m that are given in Table I under

TABLE I
RADIATION CHARACTERISTICS OF THE CRLH-LWA ANTENNA

Main beam direction θ_m of the LWA radiation pattern (°)	±10	±20	±30	±40	±50	±60
Antenna gain G_m (dB)	3.9	4.7	4.5	3.7	4.2	2.0

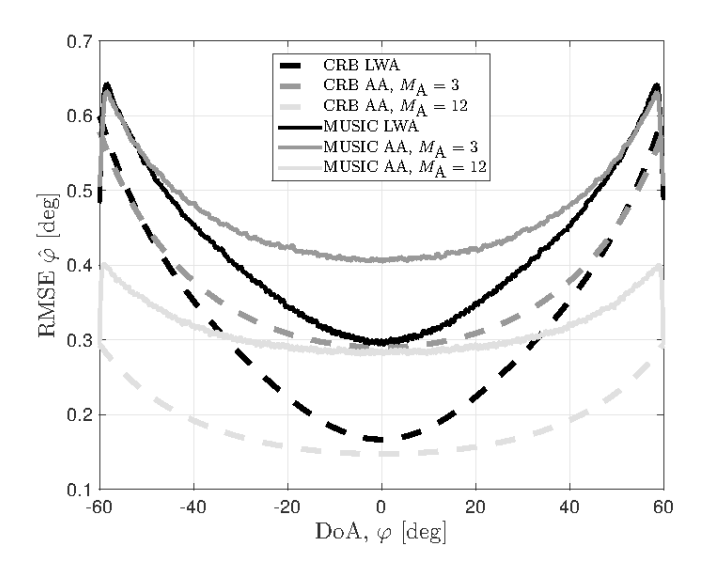


Fig. 4. Comparison of LWA with AAs with 3 and 12 antenna elements: RMSE as a function of the DoA. Parameters: SNR = 10 dB.

Section V. In all estimation cases, we use 100 complex inphase/quadrature (I/Q) samples for estimating the DoA. Note that the estimation is done prior to fast Fourier transform (FFT) processing.

Fig. 4 depicts the CRB and the simulated performance of MUSIC, with the LWA as well as with AAs, as a function of the DoA. Here, the SNR is fixed to 10 dB and the direction of the incoming signal is swept from -60° to 60° with a resolution of 0.01°. The results are averaged over 500 signal realizations for each DoA, and an additional averaging over 100 consecutive DoAs takes place for mitigating the effects of the discretized directions of the incoming signal. Based on the root-mean-squared error (RMSE) depicted in the figure, we observe that the CRB is less than 1° over the whole DoA range in all cases. Moreover, it is evident that the overall best performance is achieved with the AA consisting of $M_{\rm A}=12$ elements. However, the second best overall performance is achieved with the LWA, whereas the AA with $M_{\rm A}=3$ elements results in the worst overall performance. The simulated results, in turn, show that the MUSIC-based DoA estimation with the LWA as well as AAs has a DoA RMSE of less than 0.7° and reaches a performance close to the corresponding CRBs. In fact, it was shown in [42] that the MUSIC algorithm is asymptotically (for large N_s) unbiased. As discussed earlier, the results from [42] also apply to LWAs, as long as the steering vector is properly defined, and hence, the proposed MUSIC algorithm for LWAs is asymptotically lower-bounded by the CRB.

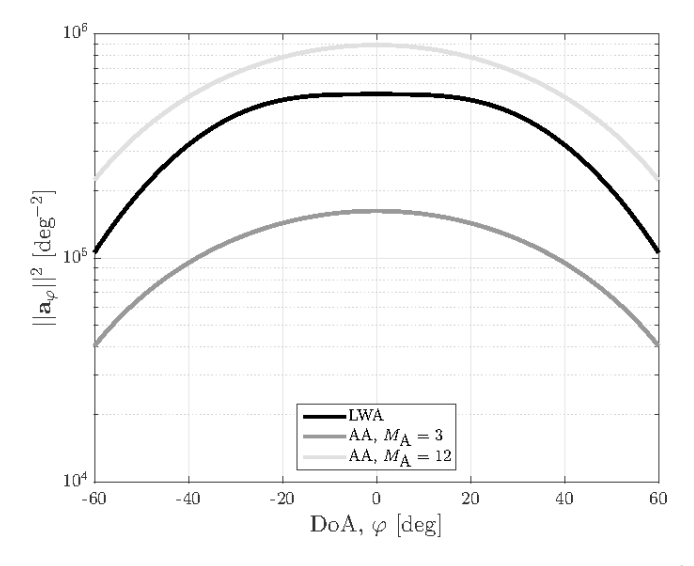


Fig. 5. Comparison of LWA with AAs: antenna-dependent component $||\mathbf{a}_{\varphi}||^2$ of the CRB in (16).

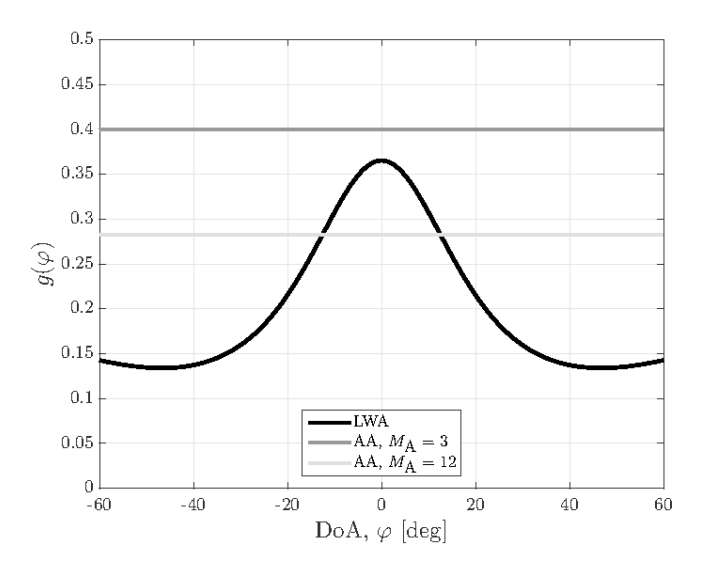


Fig. 6. Comparison of LWA with AAs: antenna-dependent component $g(\varphi)$ of the CRB in (16).

Based on the results in Fig. 4, DoAs around 0° are estimated with the highest accuracy, while the accuracy then decreases the further the DoA is from the antenna broadside. In order to understand this behavior, it is useful to realize that the CRB in (16) depends on the actual antenna only via the function $h(\varphi)$, which, in turn, can be factorized into $||\mathbf{a}||^2$ and $g(\varphi)$. The dependence of these two factors on the DoA for all three antennas and SNR = 10 dB is depicted in Figs. 5 and 6. In order to minimize the CRB, both $||\mathbf{a}_{\varphi}||^2$ and $g(\varphi)$ should be maximized. Now, $||\mathbf{a}_{\varphi}||^2 = \sum_{m=1}^{M} |[a_m]_{\varphi}|^2$ is an indication for the sensitivity of the steering vector toward changing DoAs. From Fig. 5, we see that the AA with $M_A = 12$ results in the largest $||\mathbf{a}_{\varphi}||^2$, followed by the LWA and the AA with $M_A = 3$. The observation that $||\mathbf{a}_{\varphi}||^2$ is the smallest for the AA with $M_A = 3$ is simply explained by the fact that $||\mathbf{a}_{\varphi}||^2$ increases with increasing M, i.e., the dimension of \mathbf{a} . If we were to compare the element-wise average $\overline{||a_m|_{\varphi}||^2} = \sum_{m=1}^{M} ||a_m|_{\varphi}|^2/M$, we would observe that $\overline{||a_m|_{\varphi}||^2} < ||a_{A,m}|_{\varphi}|^2$ independent

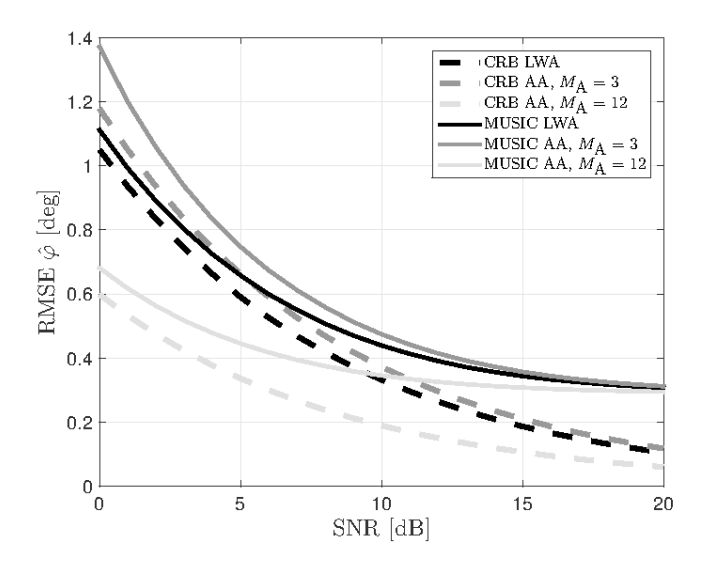


Fig. 7. Comparison of LWA with AAs with 3 and 12 antenna elements: RMSE as a function of the SNR (averaged over uniformly distributed DoA).

of M_A . Thus, on average, elements of the AA steering vector are more sensitive to changes in the DoA compared to the elements of the LWA. This is one of the reasons for the behavior of the CRBs that we have observed in Fig. 4.

Apart from the differences in the magnitude of the CRBs, we also observe that the DoA CRB of the LWA is a stronger function of the DoA itself compared with the DoA CRB of the AAs (see Fig. 4). In fact, for DoAs $\varphi \approx 0$, the LWA is performing almost as good as the AA with $M_A = 12$. As illustrated in Fig. 6, this is due to the factor $g(\varphi)$ that is a strong function of the DoA for the LWA, whereas it is independent of the DoA for the AAs.

Finally, Fig. 7 illustrates the CRB and performance of the MUSIC algorithm as a function of the SNR. Now, the SNR is swept from 0 to 20 dB with 1-dB steps. For each SNR value, we sweep the DoA from -60° to 60° with 0.01° steps. The results are averaged over all DoAs and 100 signal realizations for each SNR. Again, the AA with $M_A = 12$ elements performs the best while the LWA has the second best overall results and the array with $M_A = 3$ antennas has the worst results. With low SNRs, the differences are the highest whereas with the SNR of 20 dB the simulated performance is practically the same with all cases and the CRBs have only very small differences between each other. The difference between the simulated curves and CRBs, in turn, is caused by the discretization of the MUSIC pseudospectrum, generating a nonzero bias even for high SNR. In further simulations for selected high SNR points with an increased resolution of the pseudospectrum, we have seen that the performance of MUSIC can get arbitrarily close to the CRB. This is due to a vanishing bias with increasing resolution. We can, hence, conclude that the proposed MUSIC DoA estimator for LWAs is efficient for high SNR.

In summary, it is possible to design an AA that is capable of estimating DoAs with a better performance than the used LWA, while at the same time having similar PHY dimensions. However, such an AA would require more than $M_A = 3$ antenna elements and would thus have an increased



Fig. 8. Lobby where the measurements were carried out.

hardware complexity compared to the LWA since the AAs, especially if combined with digital beamsteering, require a complete RF chain per individual antenna element. What is also noteworthy is that we have not considered mutual coupling effects between the antenna elements in the arrays in this analysis. As is well known, the smaller the distance between antenna elements, the bigger the mutual coupling effects [43], [44]. Consequently, the mutual coupling effects would most probably affect the performance of the linear AA with $M_A = 12$ elements and thus may deteriorate the DoA estimation performance. However, it is possible to mitigate these effects using compensation methods, as is shown, e.g., in [45], also providing good operation capabilities with small antenna spacing. In practice, this would naturally require more complicated array calibration and could also increase the overall complexity of the array processing. Overall, whether an LWA is better suited for the DoA estimation than an AA is thus application-specific and boils down to a hardware-complexity/estimation-performance tradeoff. In any case, the results show that LWA type of antennas, when complemented with the digital processing and estimation algorithms proposed in this paper, can provide highly efficient and reliable DoA estimation.

V. EXPERIMENTAL SETUP

A. Indoor Environment

The performance of the proposed DoA estimation algorithms is evaluated using experimental measurements performed in an indoor environment. The experiments are carried out on the premises of Drexel University. The indoor setup, as shown in Fig. 8, is a closed lobby with stairs and glass walls. In this typical lobby setting, we anticipated both LoS components as well as non-LoS (NLoS) due to severe multipath between the transmitters (TXs) and the receivers (RXs). The layout shown in Fig. 9 depicts the arrangement of TXs and RXs in the described indoor environment. For conducting the measurements, we used three TX nodes and six RX nodes.

Each of the six RX nodes were equipped with the reconfigurable two-port CRLH-LWAs and the TXs were equipped with two standard omnidirectional antennas. We measured the lobby dimensions and transceiver antenna locations carefully with a measuring tape. In addition, LWA broadsides were steered manually toward distant reference points to obtain as precise antenna orientation information as possible. The gray

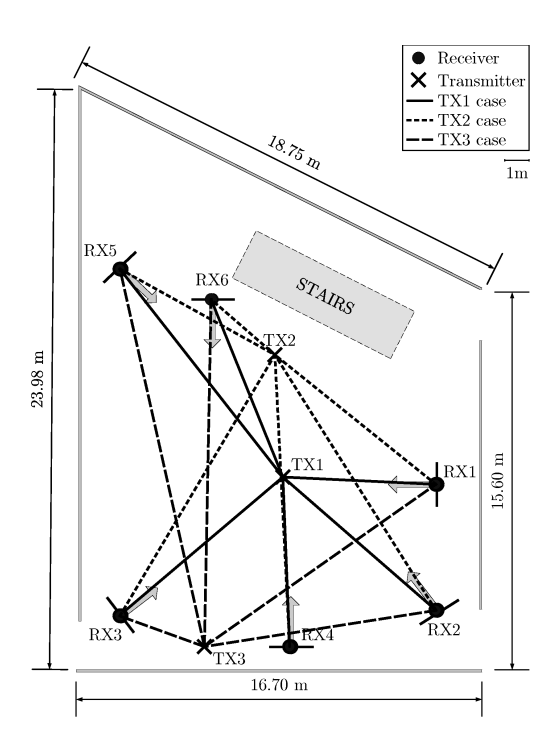


Fig. 9. Layout of the measurements. Solid black line stands for TX1, dotted black line for TX2, and dashed black line for TX3.

arrows, in Fig. 9, show the broadside direction $\theta=0^\circ$ of the RX LWAs. The real DoAs were finally calculated using basic geometry. The measurements were carried out in such a way that only one TX–RX pair was active at a time. Although we measured all TX–RX pairs, the data with TX3 were analyzed only for RX1–RX3 and RX5–RX6 since TX3–RX4 was out of the spatial scanning directions.

B. Hardware Setup and Measurement Procedure

The measurement campaign was carried out using wireless open-access research platform (WARP), a field-programmablegate-array-based software defined radio platform. Each of the TX and RX nodes was prototyped using WARP version 3 hardware and WARPLab version 7 software that is a MATLAB interface. The WARPLab interface was used to implement MIMO OFDM PHY layer code for transmission and reception of the IEEE 802.11 compliant frames. The interface was also used to centrally synchronize all the nodes, control antenna beam directions, and collect all the measurement data. The performance of the DoA estimation was evaluated in 2×2 MIMO-OFDM system with spatial multiplexing as the transmission scheme. The OFDM PHY was implemented with a total of 64 subcarriers where 48 subcarriers were used for loading data symbols, 4 for carrier frequency offset correction, and 12 empty subcarriers. The data were collected using a broadcast scheme where each designated TX broadcasts packets with binary phase shift keying as the subcarrier data modulation. After each transmission, all the RXs stored 300 packets each containing 5120 complex I/Q samples and then the antenna beam direction was switched for the next reception. The transmit power of the TX nodes was set to 15 dBm.

	TX1			TX2				TX3	STD of ϵ (°)	RMSE of ϵ (°)	
	φ (°)	φ̂ (°)	ϵ (°)	φ (°)	φ̂ (°)	ϵ (°)	φ (°)	$\hat{\varphi}$ (°)	ϵ (°)		
RX1	-3	10	13	-39	-60	-21	35	28	-7	7.0	14.8
RX2	12	-5	-17	-5	1	6	62	60	-2	11.7	10.5
RX3	3	0	-3	22	7	-15	-57	-60	-3	6.9	9.0
RX4	2	-1	-3	3	1	-2				0.7	2.5
RX5	-9	0	9	14	1	-13	-34	-56	-22	15.9	15.6
RX6	22	19	-3	49	43	-6	-1	-11	-10	3.5	7.0
STD of ϵ			10.6			9.8			9.7		
RMSE of ϵ			9.7			12.3			13.8		

TABLE III
SUMMARY OF THE DOA ESTIMATION RESULTS FOR THE PD

	TX1			TX2			TX3			STD of ϵ (°)	$ \begin{array}{c} \mathbf{RMSE} \\ \mathbf{of} \ \epsilon \ (^{\circ}) \end{array} $
	φ (°)	φ̂ (°)	ϵ ($^{\circ}$)	φ (°)	φ̂ (°)	ϵ (°)	φ (°)	φ̂ (°)	ϵ (°)		
RX1	-3	10	13	-39	60	99	35	40	5	52.1	58.0
RX2	12	-20	-32	-5	-30	-25	62	60	-2	15.7	23.5
RX3	3	10	7	22	40	18	-57	-60	-3	10.5	11.3
RX4	2	-10	-12	3	10	7				13.4	9.8
RX5	-9	-30	-21	14	10	-4	-34	-50	-16	3.5	7.0
RX6	22	30	8	49	40	-9	-1	-30	-29	12.6	17.8
STD of ϵ			18.2			44.0			16.6		
DMSE of c			17 8			42.6			15 1	i	

All the measured data were saved for offline postprocessing and evaluating the DoA estimation algorithms introduced in Section III. The DoA estimation is done before the FFT, unlike in [32] and [39] where the DoA estimation is calculated after the FFT, and it has to be calculated separately at every subcarrier. Further, the measurements were carried out in the WiFi frequency range of 2.452 GHz–2.472 C as the LWAs were calibrated for this range.

During the experiments, both the LWA's ports received the signal at the same time, thereby reducing the scanning frequency and the number of training packets by half. Antenna ports 1 and 2 collected measurements with the following 12 antenna main beam directions: -60° , -50° , -40° , -30° , -20° , -10° , 10° , 20° , 30° , 40° , 50° , and 60° , hence implying 10° resolution limit to the PD-based DoA estimation scheme. In addition, the resolution for the radiation patterns for the PPCC algorithm is set to 10° . In contrast to PD and PPCC, the resolution for the MUSIC algorithm is set to 1° . The gains of the LWA for each control voltage set are shown in Table I. In addition, we used d=1.3 cm and $\alpha=1$ in the measurement processing for the MUSIC algorithm. Moreover, we assume that only one signal is impinging to the RX, and thus set L=1.

Due to the relatively high tolerances in the current antenna manufacturing process, we did preliminary DoA estimation accuracy testing with several arbitrarily selected but known DoAs for each individual antenna. Based on the DoA estimation accuracy in these tests, we selected to use radiation patterns, which resulted in the best DoA accuracy, for the measurements under consideration. Correspondingly, the radiation patterns that caused the highest estimation errors in the preliminary testing are not used in this paper. If the antennas were manufactured in a larger scale and the manufacturing tolerances were smaller, it would be enough to test the estima-

tion accuracy only with one or very few individual antennas. Notice also that as the measurements are carried out at open WiFi frequencies with various WiFi access points within close vicinity, all WiFi traffic acts directly as cochannel interference making the measurement environment very challenging.

VI. EXPERIMENTAL RESULTS

The goal of our experimental measurements is to demonstrate and characterize LWA-based DoA estimation capabilities using the algorithms presented in Section III. Figs. 10-12 show the DoA estimation results as a function of the DoAs for the proposed single/two-port MUSIC, PD, and PPCC algorithms. The vertical lines in each plot illustrate the real DoAs for each measurement case. The figures present the best and worst DoA estimation results of the MUSIC algorithm for each TX case and corresponding DoA estimates for the PD and PPCC algorithms. DoA estimates for both the MUSIC algorithm and the power-based estimators from Section III are presented in Tables II-IV, respectively. These tables also include the individual DoA estimation errors $\epsilon_r = \hat{\varphi} - \varphi$, r = $1, \ldots, R$ for the R measurement cases, DoA estimation RMSE as well as the overall standard deviation (STD) s, calculated according to

$$s = \sqrt{\frac{1}{R - 1} \sum_{r=1}^{R} (\epsilon_r - \mu)^2}$$
 (22)

where $\mu = (1/R) \sum_{r=1}^{R} \epsilon_r$.

Based on the results, the total RMSE, calculated over all test cases, is 11.2° and the total SD is 9.8° for the MUSIC algorithm. For the PD estimator, the total RMSE is 28.6° and the total SD is 29.5° as well as the total RMSE is 16.9° and the total SD is 15.4° for the PPCC algorithm. These experimental results show that the performance of the MUSIC algorithm

	TX1			TX2				TX3	STD of ϵ (°)	$ \begin{array}{c} \mathbf{RMSE} \\ \mathbf{of} \ \epsilon \ (^{\circ}) \end{array} $	
	φ (°)	φ̂ (°)	ϵ (°)	φ (°)	$\hat{\varphi}$ (°)	ϵ (°)	φ (°)	φ̂ (°)	ϵ (°)		
RX1	-3	-10	-7	-39	-60	-21	35	60	25	17.4	19.3
RX2	12	-10	22	-5	-30	-25	62	50	-12	24.3	20.4
RX3	3	10	7	22	30	8	-57	-60	-3	6.1	6.4
RX4	2	-10	-12	3	-10	-13				0.7	12.5
RX5	-9	-30	-21	14	20	6	-34	-60	-26	17.2	19.6
RX6	22	30	8	49	50	1	-1	-30	-29	19.7	17.4
STD of ϵ			13.1			14.2			21.7		
RMSE of ϵ			14.3			14.9			21.4		

TABLE IV
SUMMARY OF THE DOA ESTIMATION RESULTS FOR THE PPCC

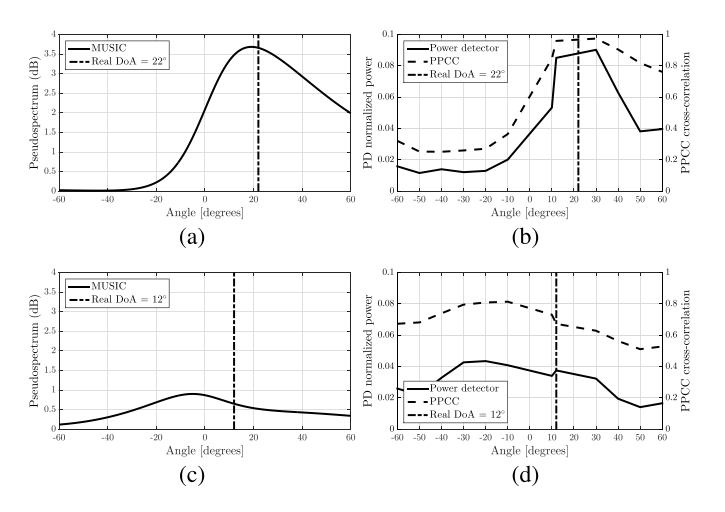


Fig. 10. DoA estimation results for the best case TX1–RX6 (top) and for the worst case TX1–RX2 (bottom). (a) and (c) Single/two-port MUSIC pseudospectrum. (b) and (d) PD and PPCC power spectrums.

is the best among these estimators. Furthermore, the PPCC algorithm also has a fairly good estimation accuracy, whereas the estimation accuracy of the PD estimator varies significantly and its performance is poor. The estimated DoAs are in good agreement with the real DoAs in the single/two-port MUSIC algorithm cases, particularly in TX1–RX6, TX2–RX4, and TX3–RX6 cases, as illustrated in Figs. 10(a), 11(a), and 12(a). However, there are significant differences in the DoA estimation accuracy in different RX locations. The significantly worst result of TX2–RX1 for MUSIC algorithm and PD estimator, as seen in Fig. 11(c) and (d), is most probably affected by harmful reflections from the stairs that are made of metal, concrete, and glass.

When the tables are analyzed column-wise, TX3 is evidently the most difficult to be estimated, as expected because of its location near the wall. Furthermore, TX1 and TX2 are easier to estimate by all RXs since they are located on very central places. We also see multiple peaks in Figs. 11(c) and (d) and 12(c) and (d). The peaks are most likely caused by the multipath effects like reflections from the stairs and walls, passersby, or WiFi traffic acting directly as cochannel interference in these measurements. For the power-based estimators, i.e., the PD and PPCC algorithms, it is intuitively clear that multipath or other signals result in additional peaks in the figures. However, in the MUSIC pseudospectrum, we also observe a peak for every individual

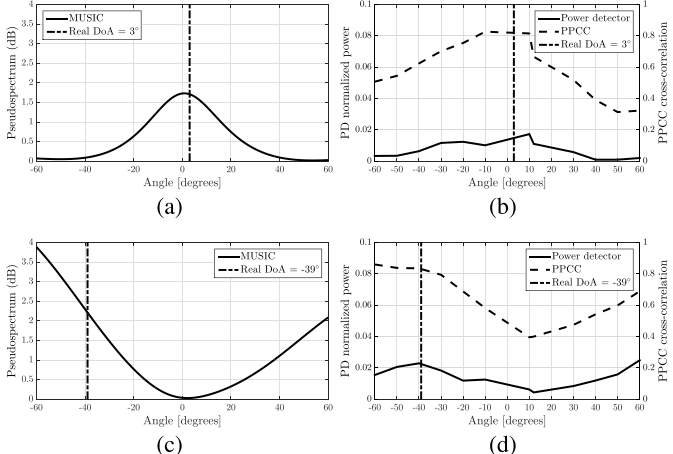


Fig. 11. DoA estimation results for the best case TX2–RX4 (top) and for the worst case TX2–RX1 (bottom). (a) and (c) Single/two-port MUSIC pseudospectrum. (b) and (d) PD and PPCC power spectrums.

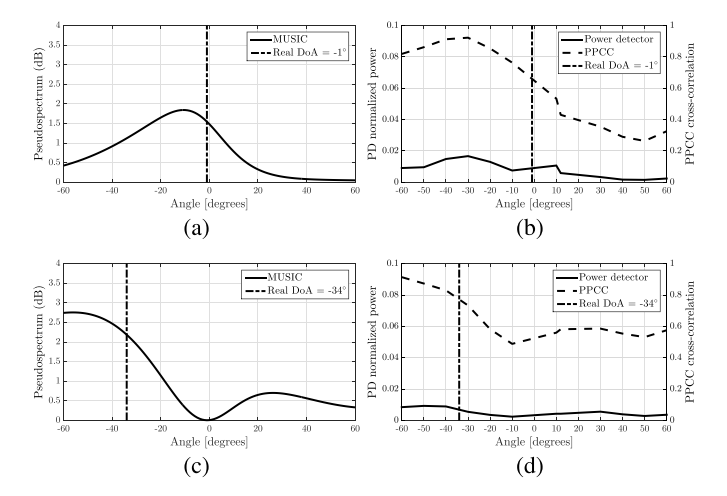


Fig. 12. DoA estimation results for the best case TX3-RX1 (top) and for the worst case TX3-RX5 (bottom). (a) and (c) Single/two-port MUSIC pseudospectrum. (b) and (d) PD and PPCC power spectrums.

incoming path or signal. This is due to the fact that, in contrast to, e.g., white noise, all paths and signals have a spatial response and therefore appear to the MUSIC algorithm much like the LoS path of the signal whose DoA we want to estimate. It is important to note that, in practice, the total number of paths or signals that we can distinguish is limited by the resolution of the antenna, which in turn is determined by the number of radiation patterns for the LWA. Therefore,

the number of peaks is still fairly small and not equal to the overall number of incoming paths and signals.

Especially in the worst result cases, the DoA estimation results for the PD and PPCC algorithms are of similar nature as with the MUSIC algorithm. If the PD estimators have no high peaks in the results or there are two or more low peaks, the MUSIC algorithm and the PPCC algorithm cannot estimate the DoA accurately. In addition, if the received signal power level is low, it is difficult to estimate the DoA. This somewhat flat response is, again, most probably caused by a weak LoS component as well as rich scattering environment causing multiple impinging non-line-of-sight (NLoS) signal paths. These phenomena can be seen in Figs. 10(c) and (d), 11(c) and (d), and 12(c) and (d).

Comparing all TX cases summarized in Tables II-IV, we note that the PD and PPCC algorithms do not yield as good results as the high-resolution MUSIC algorithm. In fact, the differences between the SDs and RMSEs are significant. This is in part explained by the discretization of the estimated DoAs. In the MUSIC variant as well as in the PPCC algorithm, the discretization is determined by the number of angles θ that we use in the calculation of (7) and (13), respectively. For the MUSIC algorithm, an increase in θ merely results in an increased computational complexity, while an increase in θ in the PPCC algorithm also requires an increased resolution in the measured LWA's radiation patterns. Finally, in order to increase the resolution of the PD algorithm, we would even have to increase the number of beam patterns as discussed also in [13]. In this paper, we used a discretization of 1° for the MUSIC variant and 10° for the power-based methods, which is also clearly reflected in the results.

Based on our observations in this section and in Section IV, we can sort the estimators by their performance in descending order as the MUSIC, PPCC, and PD algorithms. In addition to the above discussed influence of the resolution, this order can be explained by the information that we are using in each of the algorithms. In the MUSIC algorithm, we use the data from all voltage sets and use the information contained in the received signal through its spatial correlation characteristics. In the PPCC algorithm, we use data from all voltage sets, but we calculate our estimates only based on the received powers. In that way, we lose any information that we have about the signal itself. Finally, in PD, we again use only the received powers and no information about the signal itself. In addition, we also simply use the order of the powers according to their magnitude, but do not make any use of the powers themselves. In addition and in contrast to the PPCC algorithm, the information of the measured radiation pattern of a single voltage set is furthermore reduced to one value, i.e., the direction of the maximum gain.

Fig. 13 illustrates how the RX antenna would steer the main beam using the estimated DoAs of the proposed MUSIC algorithm. Solid, dashed, and dotted lines illustrate the estimated DoAs for TX1, TX2, and TX3 cases, respectively. The estimated DoAs match with the real DoAs fairly accurately in all TX cases, except for the TX1–RX2, TX1–RX5, TX2–RX1, TX2–RX3, TX3–RX5, and TX3–RX6, where the errors are significantly larger. These larger errors are most

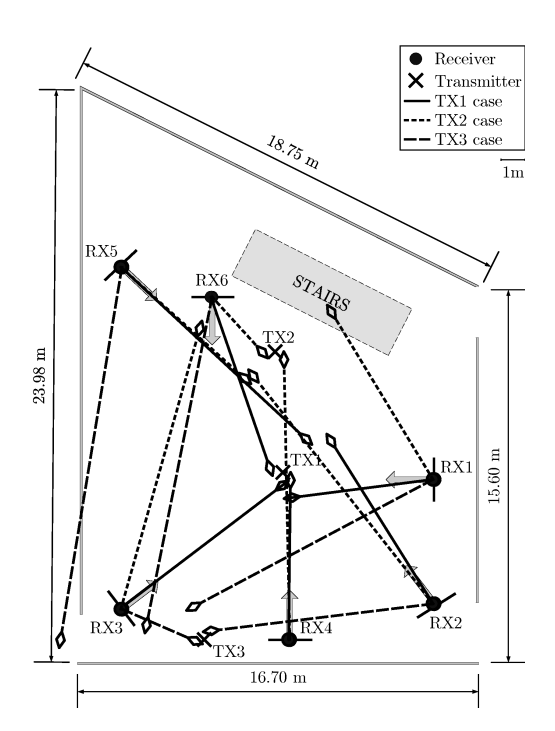


Fig. 13. DoA estimation results for the proposed MUSIC algorithm.

likely caused by severe reflections and other multipath effects, passersby, and uncontrolled cochannel WiFi traffic acting directly as external cochannel interference in the measurements. In all other cases, the differences between the real DoAs and the estimated DoAs are small, especially in the TX1 case. We conclude that the proposed MUSIC algorithm and the LWA enable fairly accurate DoA estimation, despite of the very challenging demonstration and measurement environment. Moreover, our results indicate that the considered algorithms are fairly robust to time-varying channel characteristics as our measurement setup was not optimized for fast operation, resulting in measurement times that most likely exceeded the channel coherence time.

VII. CONCLUSION

In this paper, we have explored the DoA estimation capabilities of two-port CRLH-LWAs in a real-world indoor environment. Toward that end, we first proposed modifications to two DoA estimators in order to make them suitable for LWAs. In a dedicated analysis, we have then formulated the respective CRB, and simulated and studied the performance of the MUSIC-based estimator. In addition, these results are compared to DoA estimation with conventional AAs. Finally, we have evaluated the performance of all estimators also experimentally through software-defined radio platforms equipped with CRLH-LWAs.

In detail, the results of our work are as follows. The numerical analysis revealed that the MUSIC algorithm for CRLH-LWAs is practically achieving the CRB. The comparison of the LWAs with conventional arrays shows that AAs with similar PHY dimensions exist that are capable of estimating DoAs with a better performance than LWA. However, such AAs would require more than three antenna elements and would thus have an increased hardware complexity compared

to the LWA. In addition, a compensation method would be needed to mitigate the unwanted mutual coupling effects if the antenna spacing is reduced significantly. However, such a compensation method requires more complicated array calibration methods and may also increase the overall complexity. In summary, whether an LWA is better suited for the DoA estimation than an AA is thus application-specific and boils down to a hardware-complexity/estimation-performance tradeoff.

In our experimental evaluation, we showed that the performance of DoA estimation is to some extent influenced by the heavy multipath effects present in an indoor environment. However, the results with the MUSIC variant show considerably good agreement with the real DoAs, demonstrating that DoA estimation of the received signal can be successfully performed using the two-port CRLH-LWA. Our results also show that the performance of the power-based PD and PPCC algorithms is worse than the MUSIC variant. However, at the same time, the PPCC algorithm and, in particular, the PD are also less computationally complex.

Based on our results, we conclude that the proposed MUSIC algorithm for DoA estimation along with the planar and compact LWA are effective solutions to enhance the performance of wireless communications and TX localization. In our future work, we are focusing on drastically reducing the LWA dimensions.

ACKNOWLEDGMENT

The authors would like to thank Adant Technologies Inc., Padova, Italy, for providing the antenna prototypes. The measurements have been carried out at Drexel University, Philadelphia, PA, USA. A preliminary version of this paper appeared in CROWNCOM 2013 conference [32]

REFERENCES

- [1] J. D. Boerman and J. T. Bernhard, "Performance study of pattern reconfigurable antennas in MIMO communication systems," *IEEE Trans. Antennas Propag.*, vol. 56, no. 1, pp. 231–236, Jan. 2008.
- [2] D. Piazza, N. J. Kirsch, A. Forenza, R. W. Heath, and K. R. Dandekar, "Design and evaluation of a reconfigurable antenna array for MIMO systems," *IEEE Trans. Antennas Propag.*, vol. 56, no. 3, pp. 869–881, Mar. 2008.
- [3] N. Gulati and K. R. Dandekar, "Learning state selection for reconfigurable antennas: A multi-armed bandit approach," *IEEE Trans. Antennas Propag.*, vol. 62, no. 3, pp. 1027–1038, Mar. 2014.
- [4] R. Bahl, N. Gulati, K. Dandekar, and D. Jaggard, "Impact of pattern reconfigurable antennas on Interference Alignment over measured channels," in *Proc. IEEE GLOBECOM Workshops*, Dec. 2012, pp. 557–562.
- [5] S. Begshaw, J. Chacko, N. Gulati, D. H. Nguyen, N. Kandasamy, and K. R. Dandekar, "Experimental evaluation of a reconfigurable antenna system for blind interference alignment," in *Proc. IEEE 17th Annu.* Wireless Microw. Technol. Conf. (WAMICON), Apr. 2016, pp. 1–6.
- [6] J. Werner et al., "Sectorized antenna-based DoA estimation and localization: Advanced algorithms and measurements," *IEEE J. Sel. Areas Commun.*, vol. 33, no. 11, pp. 2272–2286, Nov. 2015.
- [7] S. Abielmona, H. V. Nquen, and C. Caloz, "Analog direction of arrival estimation using an electronically-scanned CRLH leaky-wave antenna," *IEEE Trans. Antennas Propag.*, vol. 59, no. 4, pp. 1408–1410, Apr. 2011.
- [8] B. Widrow and S. D. Stearns, Adaptive Signal Processing. Englewood Cliffs, NJ, USA: Prentice-Hall, 1985.
- [9] L. C. Godara, "Application of antenna arrays to mobile communications," Part II: Beam-forming and direction-of-arrival considerations," Proc. IEEE, vol. 85, no. 8, pp. 1195–1245, Aug. 1997.
- [10] R. Baldemair et al., "Ultra-dense networks in millimeter-wave frequencies," IEEE Commun. Mag., vol. 53, no. 1, pp. 202–208, Jan. 2015.

- [11] D1.4 Channel Models, METIS, Feb. 2015. [Online]. Available: https://www.metis2020.com/wp-content/uploads/METIS_D1.4_v3.pdf
- [12] A. Hakkarainen, J. Werner, M. Costa, K. Leppanen, and M. Valkama, "High-efficiency device localization in 5G ultra-dense networks: Prospects and enabling technologies," in *Proc. IEEE 82nd Veh. Technol. Conf. (VTC Fall)*, Sep. 2015, pp. 1–5.
- [13] J. Werner, J. Wang, A. Hakkarainen, M. Valkama, and D. Cabric, "Primary user localization in cognitive radio networks using sectorized antennas," in *Proc. 10th Annu. Conf. Wireless Demand Netw. Syst.* Services (WONS), Mar. 2013, pp. 155–161.
- [14] J. D. Kraus and R. J. Marhefka, Antennas for All Applications. 3rd ed. Boston, MA, USA: McGraw-Hill, 2001.
- [15] C. A. Balanis, Antenna Theory: Analysis and Design. 3rd ed., Hoboken, NJ, USA: Wiley, 2005.
- [16] P. Gardner, M. R. Hamid, P. S. Hall, J. Kelly, F. Ghaneml, and E. Ebrahim, "Reconfigurable antennas for cognitive radio: Requirements and potential design approaches," in *Proc. Inst. Eng. Technol. Semi*nar Wideband, Multiband Antennas Arrays Defence Civil Appl., 2008, pp. 89–94.
- [17] C. Caloz and T. Itoh, Electromagnetic Metamaterials Transmission Line Theory and Microwave Applications. Hoboken, NJ, USA: Wiley, 2006.
- [18] J. R. de Luis and F. de Flaviis, "A reconfigurable dual frequency switched beam antenna array and phase shifter using PIN diodes," in Proc. IEEE Antennas Propag. Soc. Int. Symp., Jun. 2009, pp. 1–4.
- [19] C. T. P. Song, A. Mak, B. Wong, D. George, and R. D. Murch, "Compact low cost dual polarized adaptive planar phased array for WLAN," *IEEE Trans. Antennas Propag.*, vol. 53, no. 8, pp. 2406–2416, Aug. 2005.
- [20] M. Abdalla, "A planar electronically steerable patch array using tunable PRI/NRI phase shifters," *IEEE Trans. Microw. Theory Techn.*, vol. 57, no. 3, pp. 531–541, Feb. 2009.
- [21] S. Lim, C. Caloz, and T. Itoh, "Electronically scanned composite right/left handed microstrip leaky-wave antenna," *IEEE Microw. Wireless Compon. Lett.*, vol. 14, no. 6, pp. 277–279, Jun. 2004.
- [22] D. Piazza, D. Michele, and K. R. Dandekar, "Two port reconfigurable CRLH leaky wave antenna with improved impedance matching and beam tuning," in *Proc. 3rd Eur. Conf. Antennas Propag.*, 2009, pp. 2046–2049.
- [23] D. Piazza and M. D'Amico, "Metamaterial reconfigurable antennas," U.S. Patent 9196970 B2, Nov. 24, 2015.
- [24] R. O. Schmidt, "Multiple emitter location and signal parameter estimation," in *Proc. RADC Spectr. Estimation Workshop*, 1979, pp. 243–258.
- [25] K. C. Huarng and C. C. Yeh, "A unitary transformation method for angle-of-arrival estimation," *IEEE Trans. Signal Process.*, vol. 39, no. 4, pp. 975–977, Apr. 1991.
- [26] M. D. Zoltowski, G. M. Kautz, and S. D. Silverstein, "Beamspace root-MUSIC," *IEEE Trans. Signal Process.*, vol. 41, no. 1, pp. 344, Jan. 1993.
- [27] M. Haardt and J. A. Nossek, "Unitary ESPRIT: How to obtain increased estimation accuracy with a reduced computational burden," *IEEE Trans. Signal Process.*, vol. 43, no. 5, pp. 1232–1242, May 1995.
- [28] R. Roy, "ESPRIT: Estimation of signal parameters via rotational invariance techniques," Ph.D. dissertation, Stanford Univ., Stanford, CA, USA, 1987
- [29] S. Sugiura, "A review of recent patents on reactance-loaded reconfigurable antennas," *Recent Patents Elect. Eng.*, vol. 2, no. 3, pp. 200–206, Nov. 2009.
- [30] B. Friedlander and A. J. Weiss, "Eigenstructure methods for direction finding with sensor gain and phase uncertainties," in *Proc. Int. Conf. Acoust., Speech, Signal Process. (ICASSP)*, vol. 5. Apr. 1988, pp. 2681–2684.
- [31] J. P. Daniel, "Mutual coupling between antennas for emission or reception-application to passive and active dipoles," *IEEE Trans. Antennas Propag.*, vol. AP-22, no. 3, pp. 347–349, Mar. 1974.
- [32] H. Paaso, A. Mämmelä, D. Patron, and K. R. Dandekar, "Modified MUSIC algorithm for DoA estimation using CRLH leaky-wave antennas," in *Proc. 8th Int. Conf. Cognit. Radio Oriented Wireless Netw. (CROWNCOM)*, Jul. 2013, p. 166–171.
- [33] X. Yu and H. Xin, "Direction of arrival estimation utilizing incident angle dependent spectra," in *IEEE MTT-S Int. Microw. Symp. Dig.*, Jun. 2012, pp. 1–3.
- [34] J. Werner, J. Wang, A. Hakkarainen, M. Valkama, and D. Cabric, "Primary user DoA and RSS estimation in cognitive Radio networks using sectorized antennas," in *Proc. 8th Int. Conf. Cognit. Radio Oriented Wireless Netw. (CROWNCOM)*, Jul. 2013, pp. 43–48.

- [35] V. Vakilian, J. F. Frigon, and S. Roy, "Direction-of-arrival estimation in a clustered channel model," in *Proc. IEEE 10th Int. New Circuits Syst. Conf.*, Jun. 2012, pp. 313–316.
- [36] V. Vakilian, H. V. Nguyen, S. Abielmona, S. Roy, and J. F. Frigon, "Experimental study of direction-of-arrival estimation using reconfigurable antennas," in *Proc. IEEE 27th Can. Conf. Electr. Comput. Eng. (CCECE)*, May 2014, pp. 1–4.
- [37] C. Plapous, J. Cheng, E. Taillefer, H. Akifumi, and T. Ohira, "Reactance-domain MUSIC for ESPAR antennas," in *Proc. IEEE 33rd Eur. Microw. Conf.*, Oct. 2003, pp. 793–796.
- [38] S. Akkar and A. Gharsallah, "Reactance domains unitary MUSIC algorithms based on real-valued orthogonal decomposition for electronically steerable parasitic array radiator antennas," *IET Microw., Antennas Propag.*, vol. 6, no. 2, pp. 223–230, Jan. 2012.
- [39] D. Patron, H. Paaso, A. Mämmelä, D. Piazza, and K. R. Dandekar, "Improved design of a CRLH leaky-wave antenna and its application for DoA estimation," in *Proc. IEEE-APS Topical Conf. Antennas Propag. Wireless Commun. (APWC)*, Sep. 2013, p. 1343–1346.
- [40] E. Taillefer, A. Hirata, and T. Ohira, "Direction-of-arrival estimation using radiation power pattern with an ESPAR antenna," *IEEE Trans. Antennas Propag.*, vol. 53, no. 2, pp. 678–684, Feb. 2005.
- [41] S. M. Kay, "Fundamentals of statistical signal processing," in *Estimation Theory*, vol. 1, 1st ed. Englewood Cliffs, NJ, USA: Prentice-Hall, 1993.
- [42] P. Stoica and N. Arye, "MUSIC, maximum likelihood, and Cramer-Rao bound," *IEEE Trans. Acoust., Speech Signal Process.*, vol. 37, no. 5, pp. 720–741, May 1989.
- [43] H. Singh, H. L. Sneha, and R. M. Jha, "Mutual coupling in phased arrays: A review," *Int. J. Antennas Propag.*, vol. 2013, Mar. 2013, Art. no. 348123.
- [44] I. J. Gupta and A. Ksienski, "Effect of mutual coupling on the performance of adaptive arrays," *IEEE Trans. Antennas Propag.*, vol. AP-31, no. 5, pp. 785–791, Sep. 1983.
- [45] Y. Yu, H.-S. Lui, C. H. Niow, and H. T. Hui, "Improved DOA estimations using the receiving mutual impedances for mutual coupling compensation: An experimental study," *IEEE Trans. Wireless Commun.*, vol. 10, no. 7, pp. 2228–2233, Jul. 2011.



Henna Paaso received the M.Sc. and Lic.Sc. degrees from the Department of Electrical and Information Engineering, University of Oulu, Oulu, Finland, in 2005 and 2013, respectively.

She was with Drexel University, Philadelphia, PA, USA, from 2012 to 2013. She has been a Research Scientist with the VTT Technical Research Center of Finland, Oulu, since 2005. She has authored or co-authored several international publications in her fields of her expertise. Her current research interests include beamforming and direction of arrival algo-

rithms with conventional antenna arrays and leaky-wave antennas in small cell networks.



Nikhil Gulati (M'05) received the B.Eng. degree in electronics instrumentation and control from the University of Rajasthan, Jaipur, India, in 2005, and the M.S. and Ph.D. degrees in electrical engineering from Drexel University, Philadelphia, PA, USA, in 2007 and 2015, respectively, where he conducted research on sensor networks, autonomous systems, and real-time control.

From 2007 to 2010, he was a Software Engineer in a KPMG (financial service company). Currently, he is a Staff Data Scientist with GE Digital, where

he was involved in the development of analytics and machine learning frameworks for industrial Internet-of-Things applications. His previous research interests included developing online learning algorithms for exploring pattern diversity in wireless systems employing electrical reconfigurable antennas. He developed online learning algorithms for optimizing link metrics for single user and multiuser wireless networks employing interference alignment. He has authored or co-authored several patents and scientific papers in the field of reconfigurable antennas state selection, DoA estimation, interference alignment, and physical layer security.



Damiano Patron (S'11–M'15) received the B.S. degree in electronics engineering from the University of Padua, Padua, Italy, in 2010, and the M.S. and Ph.D. degrees in electrical and computer engineering from Drexel University, Philadelphia, PA, USA, in 2013 and 2015, respectively.

From 2002 to 2010, he was a System Integrator of RFID Systems with Euro-Link S.r.l. In 2010, he joined the startup company Adant Technologies Inc., Padua, as an RF and Antenna Engineer, where

he was involved in designing reconfigurable antennas for WiFi and RFID applications. From 2015 to 2017, he was a Staff Scientist with Witricity Corporation, where he was involved in new wireless charging technologies. Currently, he is a Hardware Engineer for Verily, a life science division of Google. His previous research interests included the design of reconfigurable antennas for throughput maximization and DoA estimation in wireless networks. He was involved in the development of wearable sensors and power harvesting systems. He has authored or co-authored several patents and scientific papers in the field of reconfigurable antennas, antennas miniaturization, and wearable technologies.

Dr. Patron was a recipient of several awards, including the Young Scientist Best Paper Award at the ICEAA IEEE APWC EMS Conference in 2013 and the First Prize for the Rectenna Spinout Contest at the 9th Annual IEEE International Conference on RFID in 2015.



Aki Hakkarainen received the M.Sc. degree (with Hons.) in communication electronics and the Ph.D. degree from the Tampere University of Technology (TUT), Tampere, Finland, in 2007 and 2017, respectively.

From 2007 to 2009, he was an RF Design Engineer with Nokia, Salo, Finland. From 2009 to 2011, he was a Radio System Specialist with Elisa, Tampere. In 2011, he joined the Department of Electronics and Communications Engineering, TUT. Currently, he is a Systems Specialist with Patria Aviation Oy,

Tampere. His previous research interests included digital signal processing methods for flexible radio transceivers with hardware imperfections, and directional antennas in 5G networks with an emphasis on radio localization aspects.



Janis Werner was born in Berlin, Germany, in 1986. He received the Dipl. Ing. degree in electrical engineering from the Dresden University of Technology, Dresden, Germany, in 2011, and the Ph.D. degree in electrical engineering from the Tampere University of Technology, Tampere, Finland, in 2015.

His current research interests include localization and smart antennas.



Kapil R. Dandekar (S'95–M'01–SM'07) received the B.S. degree in electrical engineering from the University of Virginia, Charlottesville, VA, USA, in 1997, and the M.S. and Ph.D. degrees in electrical and computer engineering from the University of Texas at Austin, Austin, TX, USA, in 1998 and 2001, respectively.

In 1992, he was with the U.S. Naval Observatory, Washington, DC, USA. From 1993 to 1997, he was with the U.S. Naval Research Laboratory, Washington, DC, USA. In 2001, he joined the Electrical and

Computer Engineering Department, Drexel University, Philadelphia, PA, USA, where he is currently a Professor in Electrical and Computer Engineering, the Director with the Drexel Wireless Systems Laboratory (DWSL), and an Associate Dean for Research and Graduate Studies with the Drexel University College of Engineering. His current research interests include wireless, ultrasonic, and optical communications, reconfigurable antennas, and smart textiles.

Dr. Dandekar was a member of the IEEE Educational Activities Board and Co-Founder of the EPICS-in-IEEE Program.



Mikko Valkama (S'00–M'01–SM'15) was born in Pirkkala, Finland, in 1975. He received the M.Sc. and Ph.D. degrees (both with Hons.) in electrical engineering from the Tampere University of Technology (TUT), Tampere, Finland, in 2000 and 2001, respectively.

In 2003, he was a Visiting Post-Doctoral Research Fellow with the Communications Systems and Signal Processing Institute, San Diego State University, San Diego, CA, USA. Currently, he is a Full Professor and the Laboratory Head with the

Laboratory of Electronics and Communications Engineering, TUT. His current research interests include radio communications, communications signal processing, estimation and detection techniques, signal processing algorithms for flexible radios, cognitive radio, full-duplex radio, radio localization, and 5G mobile cellular radio networks.

Dr. Valkama was a recipient of the Best Ph.D. Thesis-Award by the Finnish Academy of Science and Letters in 2002 for his dissertation entitled Advanced I/Q Signal Processing for Wideband Receivers: Models and Algorithms.



Aarne Mämmelä (M'83–SM'99) received the D.Sc. (Tech.) (with Hons.) degree from the University of Oulu, Oulu, Finland, in 1996.

He was with the University of Oulu from 1982 to 1993. He was with the University of Kaiserslautern, Kaiserslautern, Germany, from 1990 to 1991 and the University of Canterbury, Christchurch, New Zealand, from 1996 to 1997. Since 1993, he has been with the VTT Technical Research Center of Finland, Oulu. Since 1996, he has been a Research Professor of

Digital Signal Processing in Wireless Communications. Since 2004, he has been a Docent (equivalent to Adjunct Professor) with the University of Oulu. His current research interests include adaptive and learning systems and resource efficiency in telecommunications.

Dr. Mämmelä is a Technical Editor of the IEEE Wireless Communications and a member of the Research Council of Natural Sciences and Engineering in the Academy of Finland, which is funding basic research. He has given lectures on research methodology at the University of Oulu for over 15 years, including the systems approach in addition to the conventional analytical approach.